Int J Adv Manuf Technol (2007) 32: 1134–1143
DOI 10.1007/s00170-006-0436-3

ORIGINAL ARTICLE

S. H. Yoon · J. R. Hwang · S. J. Na

A study on the plasma-augmented laser welding for small-diameter STS tubes

Received: 16 May 2005 / Accepted: 14 November 2005 / Published online: 11 April 2006

Abstract Laser welding is an effective method to join small, thin parts, such as small stainless steel tubes. Laser power can be precisely adjusted to melt only a small part of the tubes, and the heat-affected zone can be controlled accurately. But laser welding systems are generally expensive; therefore, the welding speed is restricted by the maximal laser power capacity. Also, the laser welding method is very sensitive to the joint clearance and tolerance, and this makes laser welding difficult to obtain consistent welding qualities over time. Recently, solutions of these problems are being tried by introducing another heat source, such as a plasma arc. Additional plasma arc energy can make the overall welding speed faster, and sensitivity to the joint clearance can be reduced by the plasma arc. Plasma-augmented laser welding (PALW) is one of this kind of welding method, where a plasma arc is used to augment the laser welding. In this study, plasma arc welding (PAW) was added to the existing single-laser heat source to join the conventional V-grooved butt joint of thin stainless steel strips for manufacturing small-diameter stainless steel tubes. The effect of the welding speed enhancement was investigated by experiments and simulations. Finite element (FE) thermal analysis considering multiple reflections of a laser beam in the V-groove was conducted and verified.

Keywords Plasma-augmented laser welding · Plasma arc welding · Laser welding · STS tube · Small-diameter tube

S. H. Yoon
Turbopump Department, Korea Aerospace Research Institute, Daejeon, 305-333, South Korea

J. R. Hwang
Hyundai Motor Company, Ulsan, South Korea

S. J. Na (✉)
Department of Mechanical Engineering, Korea Advanced Institute of Science and Technology, Guseongdong 373-1, Yuseonggu, Daejeon, 305-701, South Korea
e-mail: sjna@kaist.ac.kr

1 Introduction

Laser welding and arc welding methods have been used in many industries for a long time, and their application is being continuously developed. Laser welding has many attractive features: laser beams can be focused to a very small diameter, and can melt only very small portions of materials. For this reason, laser welding can be conducted without affecting nearby materials, thus, the heat-affected zone (HAZ) is usually very small. This makes laser welding suitable for the precise welding of small parts. Laser beam power and profile can be adjusted or modified easily to make keyholes, thus, deep penetration welding is possible [1, 2].

In spite of these advantages, there are many difficulties encountered by laser welding to be widely used in various industries. First, the laser system is very expensive, and its cost increases exponentially as its maximal power increases. Therefore, the laser beam power is often limited by the overall system cost. Second, the laser beam diameter is usually very small, and, consequently, the welding process is very sensitive to the joint clearance and tolerance, which is probably one of the biggest problems of laser welding [3]. In most industries, there exist practical limits of clearance and tolerance on production lines, due to many reasons, which cannot be improved to a better state suitable for laser welding. Furthermore, in production lines where continuous laser beam welding is used, the clearance and vibration of the overall system make welding seam lines fluctuate. Besides, the laser welding process has many parameters, some of which are still not identified or cannot be controlled. Therefore, welding defects occur frequently and the welding results are very sensitive to the process environments.

For these difficulties of laser welding itself, there have been some efforts to solve the problems by introducing another heat source. Most of the attempts used a plasma heat source with high power lasers. An additional arc heat source enhances the total welding heat input for a relatively low cost. Also, a relatively large area of arc can eliminate or reduce the sensitivity to welding geometries, which is one

of the serious problems of laser welding alone. In most studies TIG, MIG, or plasma arc was used as a secondary heat source [4–10]. Also, a combination of CO_2 laser and a high-power diode laser was tried [11]. Recently, hybrid welding or plasma-augmented laser welding (PALW) has been broadening its area of application, and is being used for specific problems [12–14]. Also, the coaxial hybrid welding nozzle is being developed by several groups [15]. Other than these practical results, prediction of the weld pool shape in PALW was attempted [16].

In this study, a secondary plasma arc heat source was introduced to a production line of thin, small-diameter stainless steel tubes, as shown in Fig. 1. A continuous-wave CO_2 laser is used because of its ability to produce a high-power laser beam. A thin, long stainless steel strip is fed, and several forming rollers deform the strip to a cylindrical shape. Therefore, there is a continuous welding seam line, and the laser beam welds this line and the stainless steel tube is finally produced. The width and thickness of the strip is 13 mm and 0.2 mm, respectively. In this process, the laser welding speed directly affects the overall production speed, as each sequence within the production line is serially processed. For high productivity, the laser welding speed should be increased, and this means that the laser power should be increased. But the maximal laser power is limited by the system cost. Furthermore, the absorptivity of the CO_2 laser beam on metal surfaces is very low in most cases, and this makes the CO_2 laser beam welding less efficient. Besides, the strip feeding system consists of numerous rollers and guides, which tend to vibrate more at higher feeding speeds. The vibrations make the welding seam line fluctuate, and, in most cases, the small diameter of the laser beam cannot cover their fluctuation amplitudes.

For these reasons, a plasma arc was introduced as a secondary heat source to supplement the laser welding process and to reduce its disadvantages. Because the stainless steel tube is small and thin, a secondary heat source should be suitable for the joining of the tubes. For this purpose, a micro plasma arc welding (PAW) method was selected, as in Fig. 2. The torch uses pilot gas as well as shielding gas to create the pilot arc and constrict the main arc. The plasma arc can be easily started, and a highly concentrated arc is formed from the water-cooled copper nozzle. The arc dispersion angle is much smaller than that of conventional gas tungsten arc welding, and, thus, is more suitable for the welding of thin, small, and precise joints. At the same time, the heating area of the arc is larger than that of the laser beam, and, consequently, the plasma arc is not as sensitive to joint geometries [17, 18].

In this study, combination of the laser and micro PAW method was developed and the overall PALW system was implemented. Spatial configurations of the two heat sources were investigated, and the welding results were examined and compared. Finite element (FE) thermal analysis considering multiple reflections and absorptivity variation of the laser beam was conducted to predict the molten pool shapes.

2 System development

The basic idea of attaching a micro PAW torch to the existing CO_2 laser welding system is shown in Fig. 3. To minimize the modification of the laser system, the PAW torch was inclined and the angle between the two torches was fixed at about 45°. The maximal beam power of the system is 700 W, and the continuous-wave CO_2 laser beam was focused with a ZnSe lens of 125-mm focal length. The beam diameter was controlled to 0.5 mm on the surface of a workpiece. The maximal welding current of the micro plasma welding system is 80 A, where the pilot arc current has a range of 1.5 A to 2.5 A. The PAW method needs two kinds of operating gases; shielding gas and pilot gas. In this research, argon gas was used for both the shielding and pilot gases. The shielding gas flow rate was about 5 l/min, and pilot gas flow rate was about 0.5 l/min. The material used was STS304 stainless steel of 13.5-mm width and 0.2-mm thickness, which is general-purpose austenitic stainless steel.

Figure 4 shows the experimental setup of the PALW system. In the center laser, the head is positioned vertically, and the micro PAW torch is inclined with an angle of 45°. The angle and the horizontal position of the micro PAW

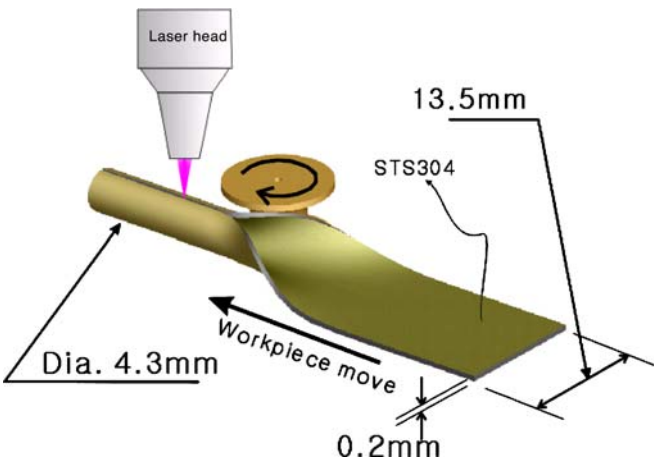

Fig. 1 Manufacturing of small-diameter stainless steel tubes

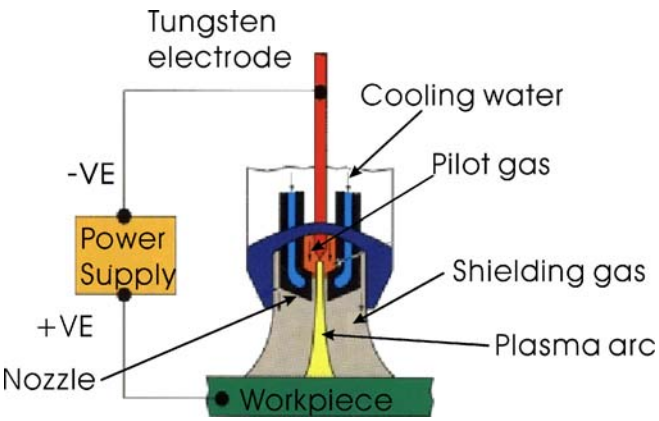

Fig. 2 Schematics of the plasma arc welding (PAW) process

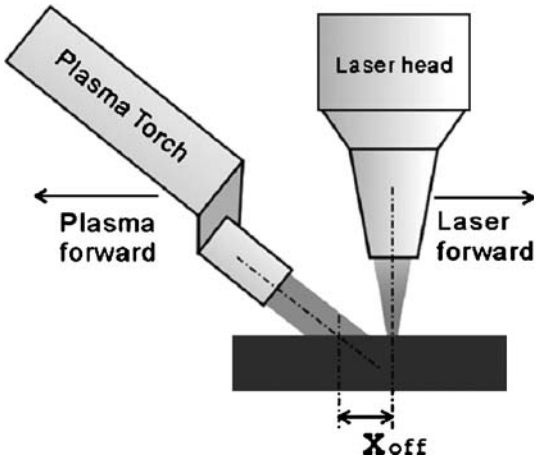

Fig. 3 Plasm-augmented laser welding (PALW) setup

torch can be adjusted by the user, but in this research, only the horizontal position was varied, while the angle was fixed to 45°. A CCD camera was installed to observe and monitor the welding process. On the XY table, a specially designed jig was placed to fix the stainless steel strips properly. The tube manufacturing process in the industry uses several forming rollers to transform strips into tubular shapes, but the tube is not closed completely. The tube seam line is slightly opened, and this gap plays a roll as a V-groove in butt welding joints, as in Fig. 5a. This V-groove enhances absorption of the laser beam by the mechanism of multiple reflections within it. To simulate this process in laboratory experiments, the jig makes two strips be positioned slightly inclined and brought into contact with each other, like conventional butt joints. The cross section of the designed jig is shown in Fig. 5b, which shows two strips inclined at an angle of 5°, and the laser beam is irradiated onto the V-groove joint. Therefore, the seam welding of small-diameter pipe can be successfully simulated by butt joint welding of thin stainless steel strips.

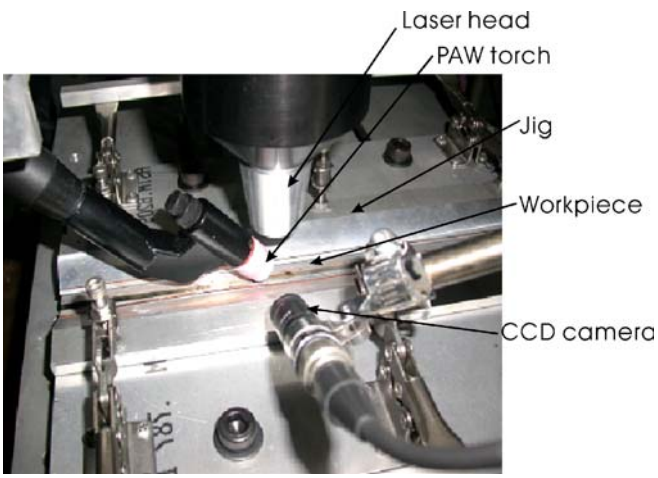

Fig. 4 Experimental setup of PALW system

3 Numerical analysis of PALW

3.1 Plasma heat source modeling

In the PALW process, there are many parameters that affect the welding results. In this study, an appropriate numerical simulation method was proposed to simulate the PALW results effectively. Among the parameters, the power and profile of the two heat sources are closely related to the welding results, and should be precisely modeled to predict the welding results reasonably. During the analysis, the plasma heat source was modeled by considering the torch angle and the effective heating area within the V-groove. Also, the laser heat source was modeled by considering multiple reflections in the V-groove.

First, the PAW heat source can be simply modeled as follows, in the case of vertical incidence:

$$I_p = \xi I_{0p} \exp\left(-c_p^2 \frac{r^2}{r_{0p}^2}\right) \quad \left[W/m^2\right] \tag{1}$$

where I_{0p} is a value depending on the voltage set at the plasma welding power source (V), the current (I), and the radius of plasma heat source (r_{0p}). It can be calculated from the plasma power, P_p, as follows:

$$I_{0p} = \frac{P_p c_p^2}{\pi r_{0p}^2} = \frac{IVc_p^2}{\pi r_{0p}^2} \tag{2}$$

where c_p is a factor of the concentration of the plasma energy within the effective radius r_{0p} and ξ is the efficiency of the plasma arc. In 1972, Arata and Miyamoto reported this value to be about 53–60%, and Metcalfe and Quigley used 60–66% for the efficiency [19, 20]. In this study, the 60% value was used as the plasma arc efficiency.

As shown in Figs. 3 and 4, the PAW torch is inclined by 45°, and, consequently, the plasma arc heat source model should be slightly modified. The projection of the heat source on the workpiece is of elliptical shape, where x_{off} means the distance between the laser heat source and the plasma heat source, as shown in Fig. 6. With this configuration, the plasma heat source can be modeled as follows, where θ_t is the tilting angle of the heat source:

$$I_p = \xi I_{0p} \sin\theta_t \exp\left[-c_p^2\left(\frac{(x - x_{off})^2}{a^2} + \frac{y^2}{b^2}\right)\right] \tag{3}$$

where the two radii of the ellipse, a and b, can be represented as follows:

$$a = \frac{r_{0p}}{\sin\theta_t} \tag{4}$$

$$b = r_{0p} \tag{5}$$

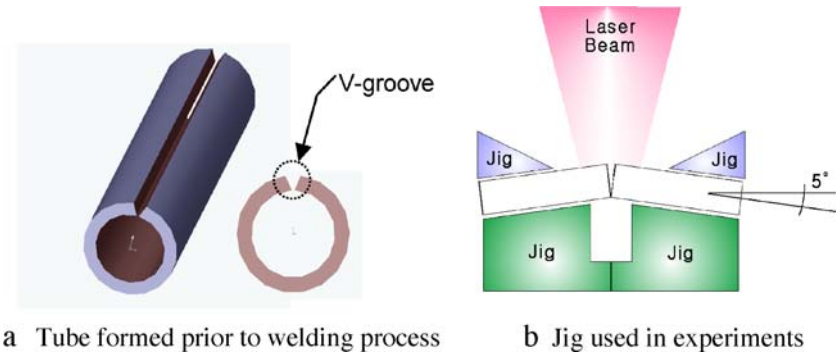

Fig. 5a, b Joint shape and jig system used in experiments. **a** Tube formed prior to welding process. **b** Jig used in experiments

The above model can be applied on a flat surface, but on the inner surface of the V-groove, the model should be modified again. In fact, the plasma itself is a kind of very complicated mass flow that is very difficult to be considered in the model. Therefore, the effect of the mass flow was neglected and the plasma was modeled as a simple Gaussian heat source with no dispersion angle. To obtain the intensity profiles of the V-groove's surface, the total power incoming to the V-groove should be obtained, which can be expressed as follows, where y_c is half-width of the V-groove entrance gap:

$$P_{gr} = 2\xi I_{0p} y_c \frac{r_{0p}\sqrt{\pi}}{c_p} \exp\left[-c_p^2\left(\frac{y_c}{2r_{0p}}\right)^2\right] \tag{6}$$

From the above equation, the maximum intensity along the welding direction is expressed as follows:

$$I_{0gr} = \frac{c\sin\theta_t}{2\omega_t r_0\sqrt{\pi}} P_{gr} \tag{7}$$

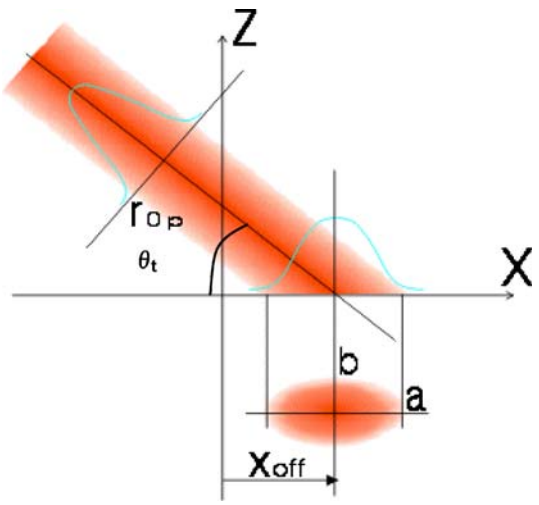

Fig. 6 Inclined Gaussian heat source

And the location of the maximum intensity is given by:

$$x_{wc} = \frac{\omega_t - \omega}{\tan\theta_t}\cos\theta_0 \tag{8}$$

where ω is a coordinate on the V-groove surface and θ_0 is a half-angle of the V-groove root.

From the above three equations, the intensity profile on the V-groove surface can be expressed as follows:

$$I_p = I_{0gr}\exp\left[-c_p^2\left(\frac{x - x_{off} - x_{wc}}{r_{0p}/\sin\theta_t}\right)\right] \tag{9}$$

Two expressions of the plasma heat source are visualized in Fig. 7.

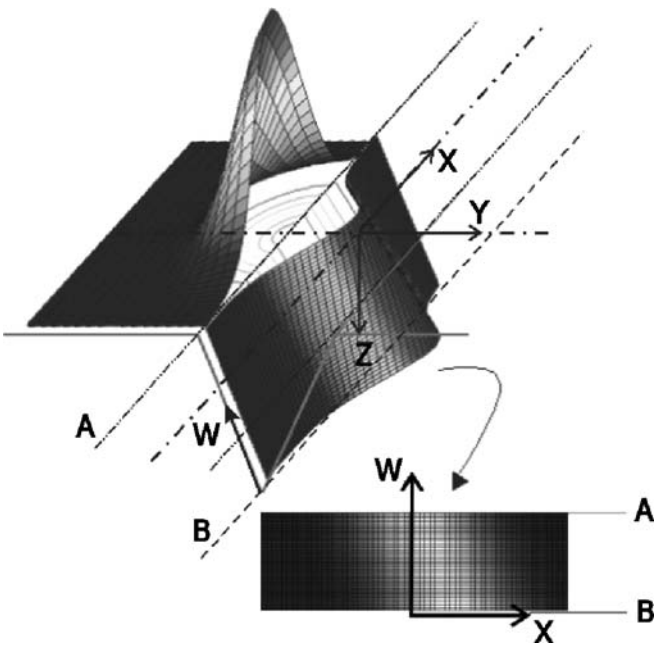

Fig. 7 Intensity profiles of the plasma heat source in and out of the V-groove

3.2 Laser heat source modeling

Laser welding is affected by various process parameters, such as the beam power, focus area, and energy distribution. In this study, a CW CO_2 laser of 680-W power was used, where the laser beam was simply modeled as a general surface heat flux as follows:

$$I(r) = I(x,\ y) = I_0 \exp\left[-c^2 \frac{r^2}{r_0^2}\right] = I_0 \exp\left[-c^2 \frac{x^2+y^2}{r_0^2}\right] \tag{10}$$

where r_0 is the 95% effective beam radius, which was set to 0.25 mm in this study.

The above model can be used for flat surfaces, but should be modified for the V-groove. Therefore, a multiple reflection model with Fresnel absorption on the V-groove surface was modeled. For this modeling, some assumptions are required to simplify the complex physical phenomena. First, the laser beam is assumed to be a straight, parallel beam with a constant effective radius of r_0. Second, the groove surface is assumed to be a mirror surface, and the absorption of beam energy by metal vapor can be neglected because the laser power is relatively low.

When the laser beam is irradiated onto a mirror surface, some portion of it is reflected, and the rest is absorbed. This is the Fresnel absorption and can be expressed as follows [21]:

$$A(\phi)=1-\frac{1}{2}\left(\frac{1+(1-\varepsilon\sin\phi)^2}{1+(1+\varepsilon\sin\phi)^2}+\frac{\varepsilon^2-2\varepsilon\sin\phi+2\sin\phi^2}{\varepsilon^2+2\varepsilon\sin\phi+2\sin\phi^2}\right) \tag{11}$$

where ε is a parameter related to the laser beam characteristics and the material. The incidence angle ϕ is the angle between the laser beam and the normal vector of the surface, but the angle θ between the laser beam and the tangent vector of the surface is defined for ease of computation. Rewriting the Fresnel absorption equation according to θ yields:

$$A(\theta)=1-\frac{1}{2}\left(\frac{1+(1-\varepsilon\cos\theta)^2}{1+(1+\varepsilon\cos\theta)^2}+\frac{\varepsilon^2-2\varepsilon\cos\theta+2\cos\theta^2}{\varepsilon^2+2\varepsilon\cos\theta+2\cos\theta^2}\right) \tag{12}$$

As shown in Fig. 8, the laser beam loses most of its energy while undergoing multiple reflections, when a parallel beam enters into the V-groove. For easier computation, the V-groove can be transformed into a set of virtual surfaces, as shown in the figure, where the beam meets several virtual surfaces. The number of surfaces met can be obtained by the following equation:

$$N_m = \frac{\pi-\theta_0}{2\theta_0} \tag{13}$$

where θ_0 is a half-angle of the V-groove. The incidence angle of the beam at the nth surface is given as follows:

$$\theta_n = (2n-1)\theta_0 \tag{14}$$

By this equation, Fresnel absorption at the nth surface is $A(\theta_n)$, and the w coordinate value w_n of the beam at the nth virtual surface is given by:

$$w_n = \frac{y}{\sin\theta_n} \tag{15}$$

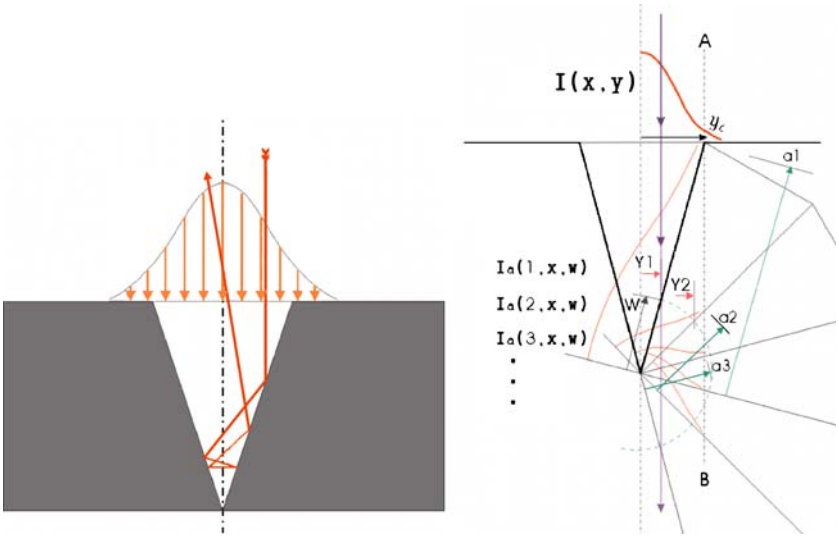

Fig. 8 Multiple reflections in the V-groove butt joint and the introduction of virtual surfaces

And the maximal values of w_n, a_n are located on the line AB as shown in Fig. 8:

$$a_n = \frac{y_c}{\sin\theta_n} \tag{16}$$

Now, some intensity functions are defined as follows:

- $I(x, y)$: intensity of the beam incoming to the groove at the (x, y) location
- $I_s(n, x, w_n)$: intensity of the incident beam at the nth reflecting surface at the (x, w_n) location
- $I_a(n, x, w_n)$: intensity of the absorbed beam at the nth reflecting surface at the (x, w_n) location
- $I_r(n, x, w_n)$: intensity of the reflected beam at the nth reflecting surface at the (x, w_n) location

It can be shown that I_s=I_a+I_r.

When a beam meets the nth wall, the absorption and reflection can be defined as follows:

$$I_a(n,\ x,\ \omega_n) = I_s(n,\ x,\ \omega_n)A(\theta_n) \tag{17}$$

$$I_r(n,\ x,\ \omega_n) = I_s(n,\ x,\ \omega_n)(1 - A(\theta_n)) \tag{18}$$

As an example, the intensity absorbed at the first wall can be expressed as:

$$I_a(1,\ x,\ \omega_1) = I(x,\ y)\sin\theta_1 A(\theta_1)u(a_1 - \omega_1) \tag{19}$$

The $u(t)$ is a unistep function.

Finally, the intensity absorbed at the nth virtual wall in the groove can be calculated with the following equation:

$$I_a(n,\ x,\ \omega_n) = I(x,\ y)\sin\theta_n A(\theta_n)\prod_{i=1}^{n-1}[1 - A(\theta_i)]u(a_n - \omega_n) \tag{20}$$

Therefore, the intensity distribution of the absorbed beams in the real V-groove wall can be found by superposition of the above equation:

$$I_A(x,\ \omega) = \sum_{n=1}^{N_m} I_a(n,\ x,\ \omega_n) \tag{21}$$

Figures 9 and 10 show the definition of the intensity functions and the steps to obtain them. Also, Fig. 11 shows the final 3D distribution of absorbed intensity in and near the V-groove.

The graph in Fig. 11b shows some discontinuous step shapes because of the superposition effect, while the maximal intensity occurs at the bottom (w=0) of the V-groove. Figure 12 shows the absorbed power efficiency

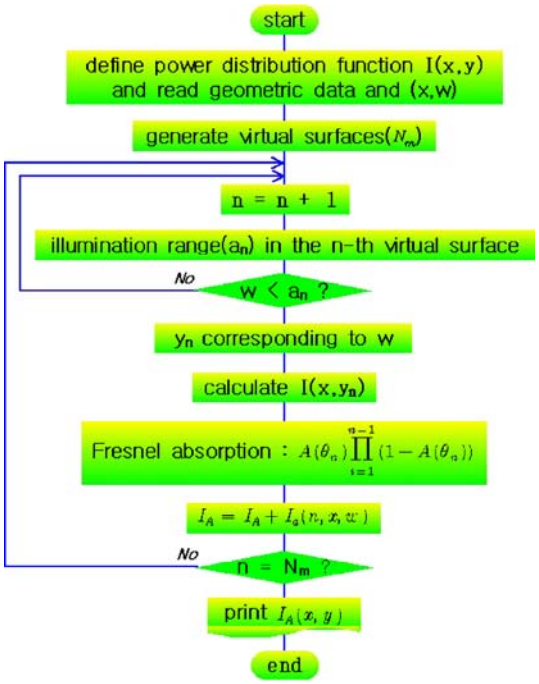

Fig. 9 Steps for the calculation of intensity functions

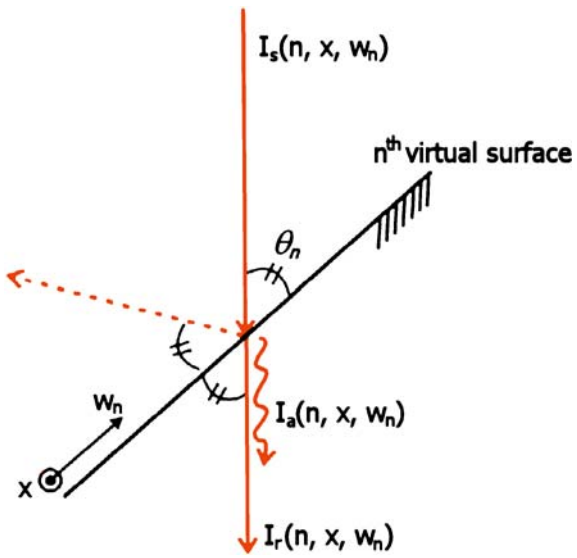

Fig. 10 Definition of the intensity functions

with respect to the groove angle. At the V-groove angle of 10°, which is the value selected in this study, the absorbed efficiency is calculated to be about 35%. The maximal efficiency can be achieved at the angle of 20°~40°. As the angle increases above this range, the efficiency is decreased to about 15%, which is almost equal to the efficiency value of the flat plate.

The multi-reflection model proposed here is valid when the V-groove wall remains at its initial geometry. But in the real situation, there occurs melting and collapse of the groove wall, which prevents the laser beam from penetrating into the bottom. For better simulation results, the

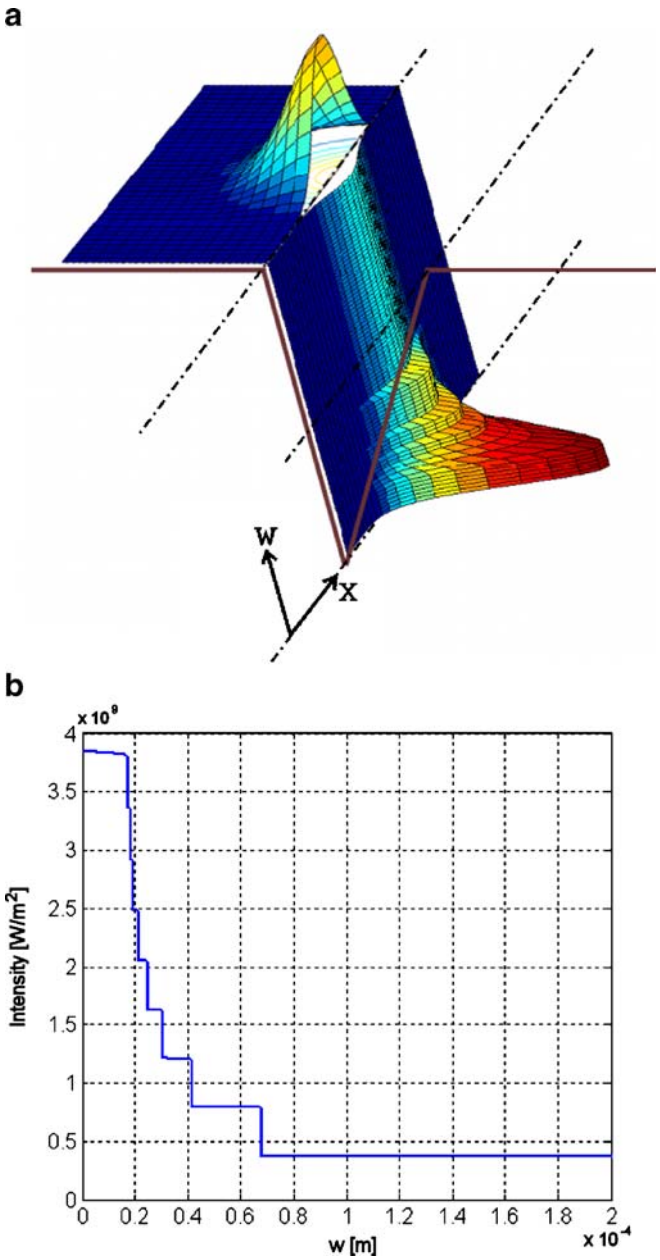

Fig. 11a, b Distribution of the absorbed intensity at the V-groove wall. **a** 3D graphical distribution. **b** 2D distribution along the *w* axis

portion of the closed groove area was determined and considered in the calculations.

Figure 13 shows the FE analysis result of the temperature prediction, assuming that there is no closing of the V-groove. In this result, it can be seen that the metal reaches its melting temperature at a point which is located $0.3r_0$ before the laser beam axis. This distance could be varied according to the feeding speed, but this value was fixed in this study for simulation simplicity. Consequently, the heat input was separated in three regions, as shown in Fig. 14. To model the groove-closing phenomena effectively, the model change method in the ABAQUS software package was used. When the groove is closed by melting and collapse, new elements were additionally created in that region.

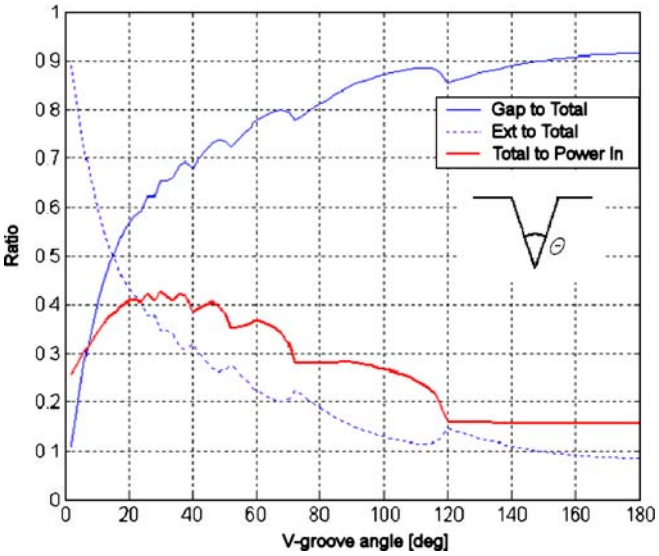

Fig. 12 Absorbed power efficiency with respect to V-groove angle

4 Experimental results

4.1 Experimental results of laser welding

The proposed analysis model was verified by welding experiments. Bead on plate welding was compared with the basic heat input model of Eq. 10, while V-groove welding was compared with the multi-reflection model of Eq. 21. The laser beam energy was fixed and only the welding speed was varied.

Fresnel absorptivity of 0.15 was applied to Eq. 10 to obtain the heat input model of bead on plate welding. Figures 15 and 16 show the laser welding results of the bead on plate welding and the V-groove butt joint.

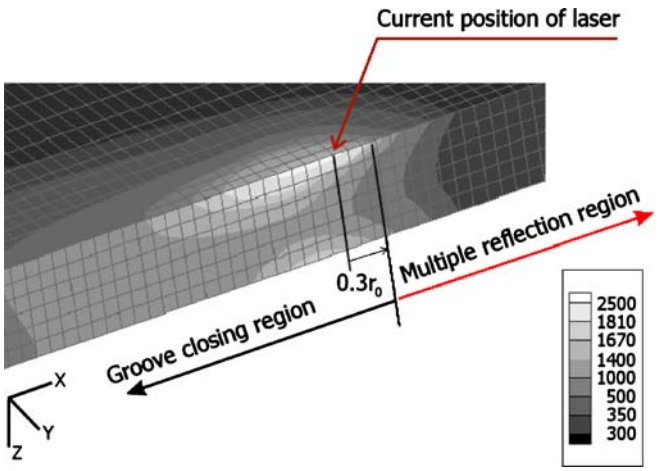

Fig. 13 Finite element (FE) analysis for determining the groove-closing region

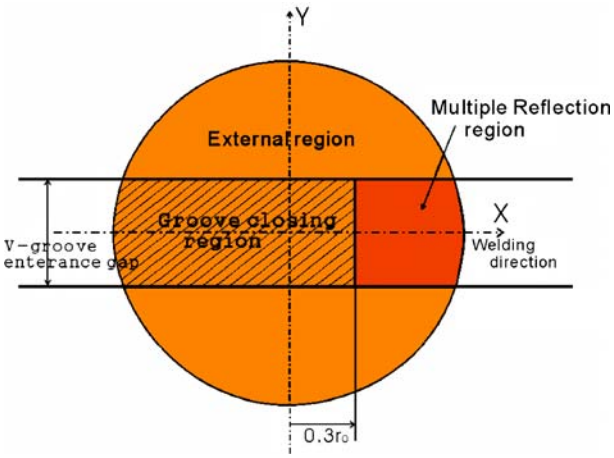

Fig. 14 Three regions for separate heat input modeling

In the results of the bead on plate welding, the analytical results showed larger molten pools than the experimental results. The reason for this is probably due to the fact that, in the analysis, the natural heat transfer coefficient of 10 W/m^{2}K was applied to the upper boundary surface, but in the real situation, the coefficient might be somewhat larger because of the forced convection effect of the shielding gas. In addition to this, there could be some heat dissipation by solid fixtures nearby. On the other hand, two results agree well in the V-groove butt welding, which implies that the absorption enhancement by the multi-reflection mechanism is somewhat larger than predicted.

4.2 Experimental results of PALW

In this section, the results of the PALW experiments and numerical analysis were compared. For the PALW heat input model, two expressions of the laser heat source and the plasma heat source were simply superposed. There have been many studies about the interaction of a laser beam and a plasma arc, where complex interactions between them are reported. In most cases, some loss of the laser beam energy by the plasma arc column is commonly known. But in this study, the loss of laser beam energy was found to be very small (less than 5%) from experiments with a calorimeter. It is thought that, for a laser beam and a plasma arc of relatively low intensities, their interactions are negligible. As a result, the intensity of the PALW can be expressed as follows:

$$I_T(x,\ y) = I_p(x,\ y) + I_A(x,\ y) \tag{22}$$

Some notations of welding directions and offset distance of the two heat sources can be found in Fig. 3. With this definition, some welding experiments were performed and the results are shown in Fig. 17. The welding speed was 12 m/min, which was notably faster than that of laser welding. The offset distance was varied from 0 mm to 5 mm. The laser beam power was fixed at 680 W, while the plasma arc current was 12 A.

The most significant tendency in the results is that the penetration depth of plasma forward welding is much larger than that of laser forward welding. This is because, in the former case, the plasma arc heat source is used auxiliary to enhance the laser heat source. In plasma forward welding, the plasma heat source preheats the welding area, and the following laser beam easily melts and welds the

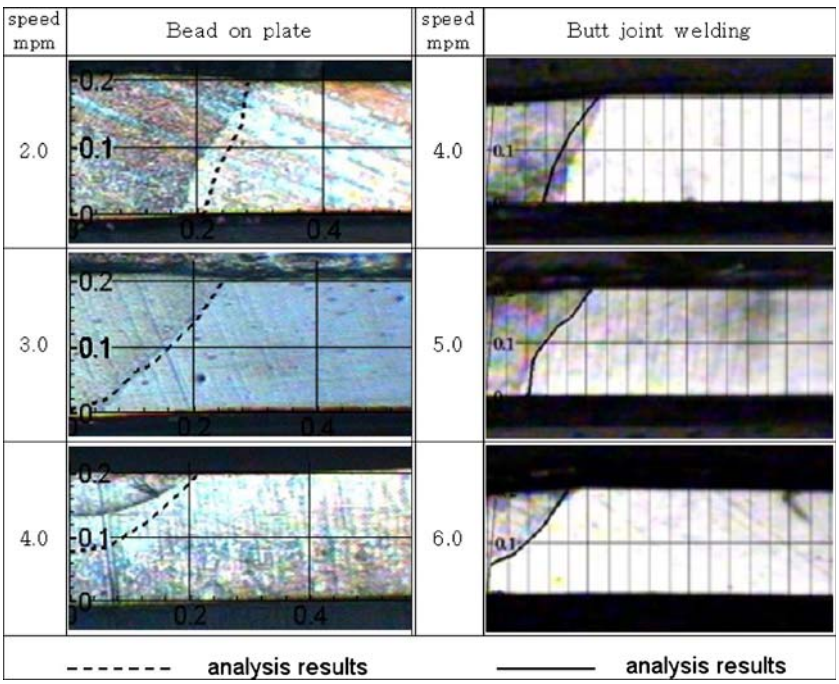

Fig. 15 Experimental and analytical results of the laser beam welding

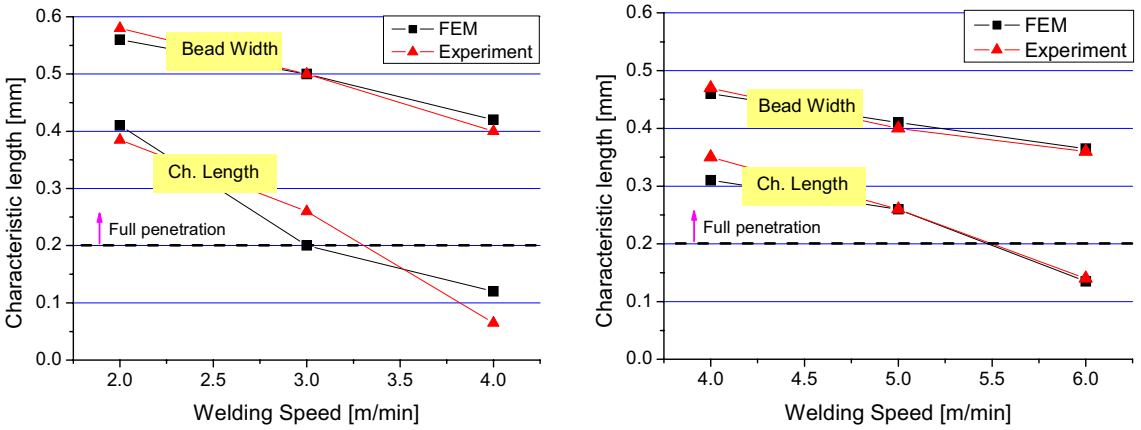

a Bead on plate b V-groove butt joint

Fig. 16a, b Weld pool geometries of the laser beam welding. **a** Bead on plate. **b** V-groove butt joint

metal with smaller beam powers. When the offset distance increases, this preheating effect weakens, and, as a result, the penetration depth also decreases.

In most hybrid welding methods that use multi-kW lasers and plasma arcs, a large bead width can be achieved by a plasma arc heat source, while central deep penetration can be achieved by a strong laser beam. Therefore, deep penetration can be retained, while tolerance of the weld seam geometry can be increased. In this study, however, most weld bead shapes showed a relatively large bead width without a deep penetration depth. The reason for this is thought that the keyhole is not generated due to low laser power, and the metal is melted by conduction mode. A relatively large surface area is melted by the plasma arc.

Another advantage of PALW is that the absorptivity of the laser beam to the preheated surface increases significantly. It is well known that the laser beam absorptivity increases as the material temperature is elevated [22]. In particular, the absorptivity of CO_2 laser beam to most metal surfaces can be dramatically enhanced by preheating, as it is very low at room temperature.

Figure 18 compares the experimental and analytical results in bead shape of the PALW process. The welding speed was 12 m/min and the offset distance 6 mm. The laser power was 680 W, while the plasma current was varied from 12 A to 20 A. In most cases, the two results are in fairly good agreement. There is a tendency that the analytical method predicts somewhat larger weld beads, which is probably due to the fact that the heat loss due to

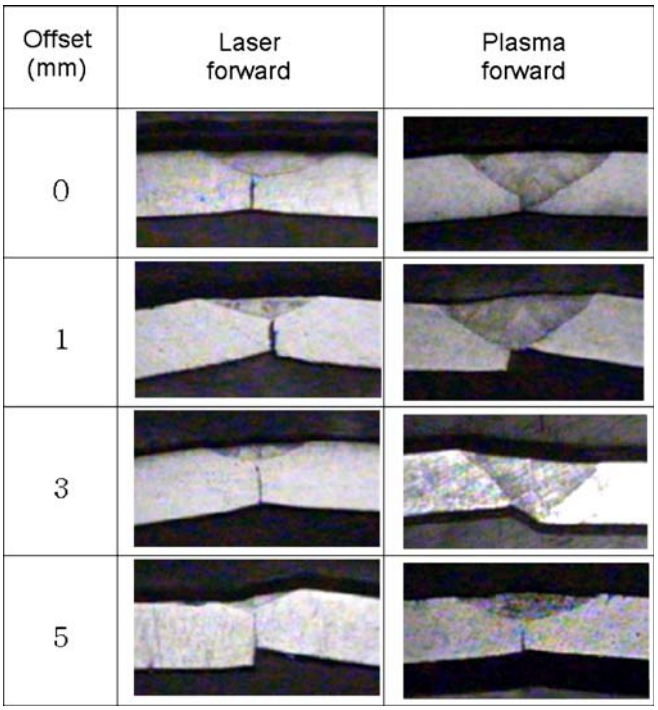

Fig. 17 Weld bead shapes for various offset distances in the PALW process

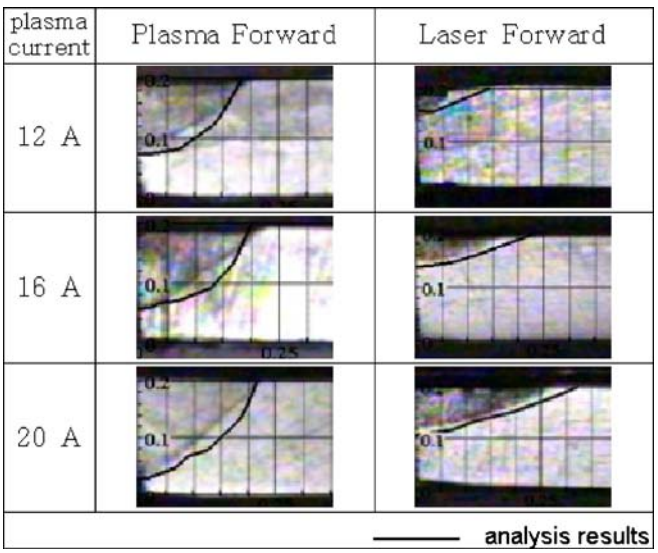

Fig. 18 Comparison of experimental and analytical results in the PALW process

the shielding gas, conduction to fixtures, and the open-groove-root shape are not considered in the analysis.

Throughout this study, it was verified that a large amount of welding speed enhancement can be achieved by introducing an auxiliary plasma arc heat source to the CO_2 laser beam welding process. It was also verified that the analytical model proposed was effective for predicting the weld bead geometry in the PALW process.

5 Conclusion

A micro plasma arc heat source was introduced as an auxiliary welding heat source to the existing CO_2 laser heat source to enhance the welding speed of small-diameter stainless steel tubes. For the prediction of the weld bead shape, an analytical model was proposed and verified by corresponding experiments. The simplified expressions for the plasma arc heat source were proved to be valid, while for the laser heat source at the V-groove wall, multiple reflections were modeled mathematically by using virtual reflecting surfaces. This model was also verified and showed a good agreement with the experiments. The welding speed was greatly enhanced in the plasma-augmented laser welding (PALW) process by at least 200% compared to the laser-only welding process. The first reason for this improvement is due to the addition of the intensities of two heat sources, and the second reason is the enhancement of laser beam absorptivity by the preheating effect of the plasma arc heat source. This absorptivity enhancement of the stainless steel for the CO_2 laser beam was also considered in the analysis to correctly predict the weld bead shape, and was also verified by the experimental results.

Acknowledgements The authors would like to thank the LS Cable Company, South Korea, for their financial support through a research grant.

References

1. Ready JF (1997) Industrial applications of lasers, 2nd edn. Academic Press, New York
2. Dawes C (1992) Laser welding. Abington, Cambridge, UK, pp 26–29
3. Girard K, Jouvard JM, Naudy PH (2000) Study of voluminal defects observed in laser spot welding of tantalum. Appl Phys 33(21):2815–2824
4. Eboo M, Steen WM (1979) Arc augmented laser welding. Met Constr 11(7):332–335
5. Matsuda J, Utsumi A, Katsumura M, Hamasaki M, Nagata S (1988) TIG or MIG arc augmented laser welding of thick mild steel plate. Join Mater 1(1):31–34
6. Gureev DM, Kanavin AP, Katulin VA, Levin AV, Nikolaev VD, Petrov AL, Satyugov VM, Stranin SA, Zaikin AE, Zolotarevskii AV (1996) Laser-arc treatment of materials and its application. J Russ Laser Res 17(6):585–606
7. Abe N, Hayashi M (2002) Trends in laser arc combination welding methods. Weld Int 16(2):94–98
8. Page CJ, Devermann T, Biffin J, Blundell N (2002) Plasma augmented laser welding and its applications. Sci Technol Weld Join 7(1):1–10
9. Ono M, Shinbo Y, Yoshitake A, Ohmura M (2002) Welding properties of thin steel sheets by laser–arc hybrid welding: laser-focused arc welding. Proc SPIE 4831:369–374
10. Kim T, Suga Y, Koike T (2003) Welding of thin steel plates by hybrid welding process combined TIG arc with YAG laser. JSME Int J 46(3):202–207
11. Bonss S, Brenner B, Beyer E (2001) Innovations in laser hybrid technology: the combination of CO_2 and high-power diode lasers offers a better surface quality and a pore-free welding seam. Ind Laser Solut Manuf 16(1):29–32
12. Hyatt CV, Magee KH, Porter JF, Merchant VE, Matthews JR (2001) Laser-assisted gas metal arc welding of 25-mm-thick HY-80 plate. Weld J 80:163–172
13. Jokinen T, Kujanpaa V (2003) High power Nd:YAG laser welding in manufacturing of vacuum vessel of fusion reactor. Fusion Eng Des 69(1–4):349–353
14. Liu L, Wang J, Song G (2004) Hybrid laser-TIG welding, laser beam welding and gas tungsten arc welding of AZ31B magnesium alloy. Mater Sci Eng 381(1–2):129–133
15. Zhang X, Chen W, Shuang Y, Wang K (2005) Coaxial hybrid CO_2-MIG welding system and its application in welding of aluminum alloys. Proc SPIE 5629:161–168
16. Vitek JM, David SA, Richey MW, Biffin J, Blundell N, Page CJ (2001) Weld pool shape prediction in plasma augmented laser welded steel. Sci Technol Weld Join 6(5):305–314
17. Lancaster JF (1986) The physics of welding, 2nd edn. Pergamon Press, New York, pp 306–325
18. Johnson KI (1985) Introduction to microjoining. Abington, Cambridge, UK, pp 1–10
19. Metcalfe JC, Quigley MBC (1975) Heat transfer in plasma-arc welding. Welding J 54(3):99–103
20. Arata Y, Miyamoto I (1972) Theoretical analysis of weld penetration due to high energy density beam. Trans JWRI 1 (1):11–16
21. Solana P, Negro G (1997) A study of the effect of multiple reflections on the shape of the keyhole in the laser processing of materials. Appl Phys 30(23):3216–3222
22. Wieting TJ, Schriempf JT (1996) Infrared absorptances of partially ordered alloys at elevated temperatures. J of Appl Phys 47(9):4009–4011